Energy 239 (2022) 122103

Contents lists available at ScienceDirect

Energy

journal homepage: www.elsevier.com/locate/energy

# Optimize heat prosumers' economic performance under current heating price models by using water tank thermal energy storage

Haoran Li [a, *], Juan Hou [a], Zhiyong Tian [b], Tianzhen Hong [c], Natasa Nord [a], Daniel Rohde [d]

[a] Department of Energy and Process Technology, Norwegian University of Science and Technology, Kolbjørn Hejes vei 1 B, Trondheim, 7491, Norway
[b] School of Environmental Science and Engineering, Huazhong University of Science and Technology, Wuhan, PR China
[c] Building Technology and Urban Systems Division, Lawrence Berkeley National Laboratory, 1 Cyclotron Road, Berkeley, CA, 94720, USA
[d] SINTEF Energy Research, Sem Sælands vei 11, 7034, Trondheim, Norway

ARTICLE INFO

*Article history:*
Received 29 March 2021
Received in revised form
19 August 2021
Accepted 19 September 2021
Available online 22 September 2021

*Keywords:*
4th generation district heating
Thermal energy storage
Distributed heat sources
Heating price model
Peak load
Mismatch problem

ABSTRACT

Due to heat prosumers' dual roles of heat producer and heat consumer, the future district heating (DH) systems will become more flexible and competitive. However, the current heating price models have not yet supported the reverse heat supply from prosumers to the central DH system, which means the prosumers would gain no economic benefit from supplying heat to the central DH system. These unidirectional heating price models will reduce interest in prosumers, and thus hinder the promotion of prosumers in DH systems. This study aimed to optimize prosumers' economic performance under the current heating price models by introducing water tank thermal energy storage (WTTES). A dynamic optimization problem was formulated to explore prosumers' economic potentials. The size parameter of WTTESs was swept in prosumers to obtain the optimal storage size considering the trade-off between the payback period and the heating cost saving. The proposed method was tested on a campus DH system in Norway. The results showed that the prosumer's annual heating cost was saved up to 9%, and the investment of WTTES could be recovered in less than ten years. This study could provide guidelines on improving prosumers' economic performance and promote the development of prosumers during the transformation period of DH systems.


## 1. Introduction

Buildings account for a large share of total energy use and contribute to global warming considerably. In the European Union (EU), buildings are responsible for approximately 40% of total energy use and 36% of greenhouse gas emissions [1]. Space heating (SH) and domestic hot water (DHW) systems, as essential parts of building energy systems, play an important role in buildings' energy use. For example, in the residential sector of the EU countries, about 80% of the energy use is for SH and DHW [2,3]. District heating (DH) systems can satisfy buildings' heat demand in an energy-efficient and environment-friendly way [4]. Due to these merits, DH systems are competitive compared with alternative heating technologies, especially for urban areas with concentrated heat demand. Currently, more than four thousand DH systems are working successfully in Europe [5], and the national heat market share for DH systems can reach 60% for some areas [6–8]. However, DH systems' competitiveness is weakened by several challenges, such as the considerable distribution heat loss caused by high distribution temperature and the shrinking heat market due to the improving building efficiency [4]. To deal with these challenges and stay competitive, the current second and third generation DH systems are transforming to the fourth and fifth generation DH systems [9–12]. The transformation includes decreasing distribution temperature and upgrading infrastructure, and hence reduces the distribution heat loss and opens the door to more free heat such as renewables and waste heats.

For the future DH systems, renewables and waste heats may be integrated into the user side as distributed heat sources (DHSs) besides the central DH system. These end-users with DHSs are called heat prosumers due to their dual roles of producer and consumer. Fig. 1 illustrates examples of heat prosumers in a DH system. The block *Individual Prosumers* in the upper right of Fig. 1 shows different types of individual prosumers that integrated into the central DH system, these prosumers maybe a building installed with solar panels, a food store with waste heat from the

* Corresponding author.
*E-mail address:* haoranli@ntnu.no (H. Li).

https://doi.org/10.1016/j.energy.2021.122103

**Nomenclature**

| | |
|---|---|
| CHP | Combine heat and power plant |
| CV(RMSE) | Coefficient of variation of the root mean square error |
| DC | Data centre |
| DH | District heating |
| DHW | Domestic hot water |
| DHS | Distributed heat source |
| EDC | Energy demand component |
| FDC | Flow demand component |
| FXC | Fixed component |
| HE | Heat exchanger |
| LDC | Load demand component |
| MS | Main substation |
| NLP | Nonlinear programming |
| NMBE | Normalized mean bias error |
| R2R | Extraction from the return line and feed into the return line |
| R2S | Extraction from the return line and feed into the supply line |
| S2S | Extraction from the supply line and feed into the supply line |
| SH | Space heating |
| TES | Thermal energy storage |
| WTTES | Water tank thermal energy storage |

refrigeration system, or a factory with waste heat from the production process. In addition, the block *Community Prosumer* in the lower right of Fig. 1 presents a community prosumer with end-users and DHSs. These end-users are a cluster of buildings that may contain residential buildings and commercial buildings, and the DHSs may be a data centre (DC) with waste heat from its cooling system and a micro combine heat and power plant (CHP). Different from the individual prosumers connecting to the central DH system directly, the community prosumer is connected to the central DH system via the main substation (MS), and hence the management of the community DH system can be separated from the central DH system. For both the individual prosumers and the community prosumers, it allows bidirectional heat flow between the prosumers and the central DH system. Therefore, the prosumers may be supplied with heat from the central DH system during high heat demand periods, and feed surplus heat from their DHSs to the central DH system during low heat demand periods.

There is a growing interest in prosumers in DH systems. Nord et al. [13] and Lickleder et al. [14] proposed methods to model heat prosumer-based DH systems. Marguerite et al. introduced a tool to optimize the design and operation of prosumers [15]. Pipiciello et al. developed a new type of substation for heat prosumers in DH systems [16]. Nielsen et al. [17], Brand et al. [18], and Gross et al. [19] investigated the impacts of prosumers on DH systems. Huang et al. reviewed the applications of DCs as prosumers in DH systems [20], and Kauko et al. studied the impacts of DCs and supermarkets as prosumers in DH systems [21]. Previous research has proposed the methods to design and operate prosumers and demonstrated the economic benefits of introducing prosumers in

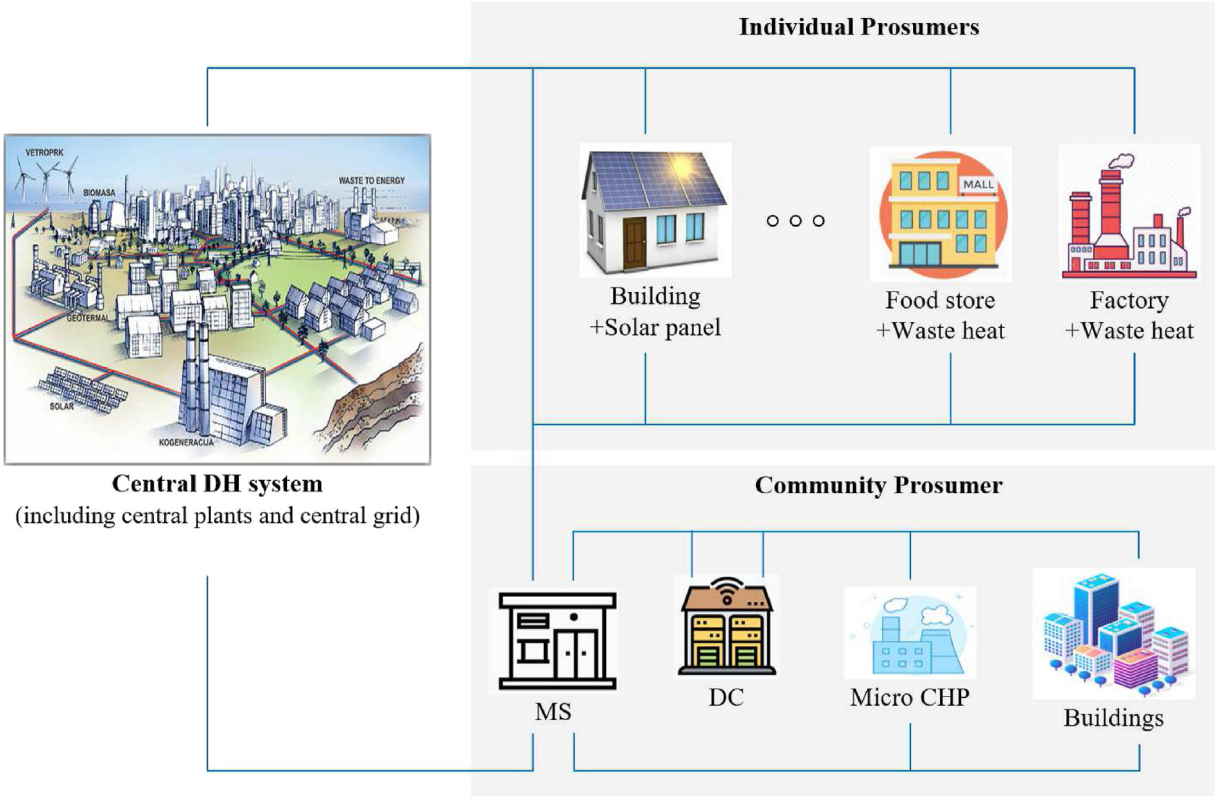


**Fig. 1.** Schematic illustrates examples of prosumers in a DH system.

DH systems. However, there is limited research focusing on optimizing prosumers' economic performance, especially under the current heating price models. During the transformation period of the DH system, despite some successful projects with bidirectional heating price models, the widely used heating price models have not supported the reverse heat supply from the heat prosumers to the central DH system, which means the prosumers would gain no economic benefit from supplying heat to the central DH system [22]. These unidirectional heating price models are reducing people's interest in heat prosumers, and thus hindering the promotion of prosumers in DH systems. Therefore, further research is needed to optimize prosumers' economic performance under the current widely used heating price models during the transformation period of the DH system.

The current widely used heating price models charge the heating cost of heat prosumers based on both the heat use and the peak load [22]. Therefore, the two possible ways to optimize heat prosumers' economic performance are: 1) increasing the self-utilization rate of heat supply from prosumers' DHSs, and hence reducing the heat supply from the central DH system, and 2) shaving prosumers' peak load by shifting parts of central DH system's heat supply from peak hours to non-peak hours. Thermal energy storages (TESs) have been proven to be good at achieving the above goals. Firstly, TESs may be used to relieve the mismatch between prosumers' heat supply from DHSs and buildings' heat demand [23–27]. Consequently, less heat is fed to the central DH system when surplus heat exists, and the self-utilization rate of the heat supply from prosumers' DHSs is increased. Secondly, TESs may shift the central DH system's heat supply from peak hours to non-peak hours, thereby shaving the peak load of the heat prosumers [28–30]. However, one barrier to the integration of TESs into prosumers is their high investment costs and the economic risk of long payback periods. Therefore, further research is needed to explore the economic feasibility of introducing TESs to prosumers under current heating price models.

This study aimed to break the above economic barrier through the optimal operation of heat prosumers with TESs and the optimal sizing of TESs. Firstly, a water tank thermal energy storage (WTTES) was chosen as short-term TES and integrated into a prosumer. Afterwards, a dynamic optimization problem was formulated aiming to explore the economic potential of the heat prosumer with TES. The economic performance of the prosumer with TES was evaluated in terms of heating cost saving and payback period. Finally, the size parameter of WTTES was swept to obtain the optimal storage size considering the trade-off between the payback period and the heating cost saving. The proposed method was tested on a campus DH system in Norway, which received heat from the central DH system, meanwhile, had its own DHS with waste heat recovery from the university DC. The main contributions of this study are summarized as the following. Firstly, the technical contribution is to support the transformation of current DH systems towards completely renewable-based DH systems with DHSs by optimizing prosumers' economic performance under the current heating price models, which is a practical but rarely addressed problem. Secondly, the scientific contribution is to use the technique of combining dynamic optimization and parameter' sweeping to explore prosumers' economic potentials considering the economic feasibility after introducing TESs. Thirdly, the practical contribution is to provide more comprehensive recommendations for heat prosumers and DH companies to understand the effect of the peak load definition on the economic performance of heat prosumers. This study provides guidelines on improving prosumers' economic performance during the transformation period of the DH system, and thus promote the development of the heat prosumers in DH systems.

The remaining of the article is organized as follows. Section 2 proposes a generalized heating price model based on the current widely used heating price models, afterwards introduces the system design and operation strategy aiming to optimize prosumers' economic performance under the generalized heating price model by using short-term TESs. Section 3 introduces the background of the case study, meanwhile provides information on research scenarios and simulation settings. Section 4 investigates and compares different scenarios' performance in terms of energy and economic indicators. Section 5 discusses the effects of the peak load definition on prosumers' economic performance and investigates the WTTESs' thermoclines during charging and discharging processes. Section 6 concludes this study.

## 2. Method

This section introduces the method to optimize prosumers' economic performance under current heating price models by using WTTESs. Firstly, a generalized heating price model is proposed based on the current widely used heating price models. Afterwards, considering the generalized heating price model, the system design for prosumers with the WTTESs and the optimization problem aiming to minimize the prosumers' heating cost are given. Meanwhile, the models and constraints used in the optimization problem are presented. Finally, the economic indicators used to evaluate prosumers' performance are introduced.

This study was based on numerical simulation. The DH system model was built using the Modelica language, which is an object-oriented language to conveniently model physical systems [31]. The optimization was performed with JModelica.org, which is an open-source platform for the simulation and optimization of complex dynamic systems [32]. For the optimization process based on the JModelica.org platform, the formulated infinite-dimensional optimization problem was transcribed into a finite-dimensional nonlinear programming (NLP) problem through Direct collocation [33]. Afterwards, the obtained NLP problem was solved by NLP solvers in the following steps. Firstly, the inequality constraints in the NLP problem were eliminated using the interior-point method [34]. Then a local optimum for the NLP was achieved by solving the first order Karush-Kuhn-Tucker condition, using iterative techniques through Newton's method.

### 2.1. Generalized heating price model

Although heating price models vary with local DH companies, a generalized heating price model was defined and was used in the optimization of prosumers' economic performance. This generalized heating price model was defined as suggested in the review paper of [22], where the current heating price models may include four components: fixed component (FXC), flow demand component (FDC), energy demand component (EDC), and load demand component (LDC). The FXC is paid to connect to the central DH system. The FDC is charged based on the volume of the hot water used to deliver heat and is intended to motivate the low return temperature. The LDC covers the DH companies' cost to maintain a certain level of capacity for the peak load, the initial investment of new facilities, depreciation, etc. It is charged based on the peak load of the end-users. The EDC covers the fuel cost and is charged based on the total heat use of end-users.

Based on the review article of [22], the existence and the average share of each component for the Swedish DH systems are illustrated in Fig. 2. About half of the heating price models include the FXC (60%) and the FDC (50%), however, they only account for 1–2% of the total heating cost. In contrast, the LDC and the EDC are the most commonly used components. About 87% of the current

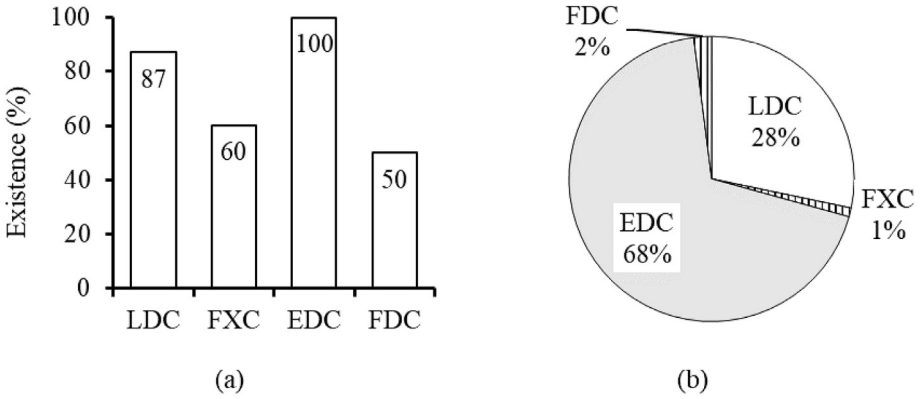


**Fig. 2.** The existence (a) and average share (b) of each component in investigated heating price models [22].

heating price models have the LDC, and all the current heating price models have the EDC. They together account for 96% of the total heating cost. There are technical-economic reasons for the configuration of a heating price model. All the DH companies want to cover their production cost and therefore the EDC is always included. For newer DH companies that may be oversized than the current heat demand, the most important component to charge the customers is the EDC. In addition, for existing DH companies that may have issues in further capacity increase, more effective utilization of the existing capacities is crucial and therefore the LDC is becoming very important and valuable. According to the above discussion, a generalized heating price model was proposed considering only the LDC and EDC as shown in Equation (1). The introduced generalized heating price model is just a theoretical suggestion and DH companies may organize their models based on their needs.

$$C_{tot} = C_{ldc} + C_{edc} \tag{1}$$

where $C_{tot}$ is the total heating cost, $C_{ldc}$ is the LDC, and $C_{edc}$ is the EDC.

The LDC, $C_{ldc}$, was calculated as Equation (2):

$$C_{ldc} = LP \cdot \dot{Q}_{pea} \tag{2}$$

where $LP$ is the LDC heating price, and $\dot{Q}_{pea}$ is the yearly peak load according to Refs. [35,36].

The EDC, $C_{edc}$, was calculated as Equation (3):

$$C_{edc} = \int_{t_0}^{t_f} EP(t) \cdot \dot{Q}(t) dt \tag{3}$$

where $\dot{Q}(t)$ is the heat flow rate supplied to the heat user and $EP(t)$ is the EDC heating price.

### 2.2. System design for a heat prosumer with WTTES

As introduced in Section 1, WTTES may be integrated into a heat prosumer to improve the economic performance of the heat prosumer under the current heating price models. Fig. 3 illustrates the proposed system design for a prosumer with WTTES, which may increase the self-utilization rate of the heat supply from the prosumer's DHSs and shave the prosumer's peak load. In the system, the DHS may be low-temperature heat sources from renewables or waste heat. There are mainly three configurations to integrate the DHSs into DH grids: 1) extraction from the return line and feed into the supply line (R2S), 2) extraction from the return line and feed into the return line (R2R), and 3) extraction from the supply line and feed into the supply line (S2S). In this study, the R2R mode was chosen, because it is preferable for low-temperature heat sources [4].

In addition, the MS connects the prosumer with the central DH system. The heat exchanger 1 (HE1) in the MS is connected to the TES and used for the heat charging of the WTTES. During the warm period with lower heat demand, the HE1 may supplement the heat supply from the prosumer's DHS. During the cold period with higher heat demand, the HE1 contributes to the peak load shaving, because it may charge the TES at non-peak hours and thus the stored heat can be used at peak hours. Heat exchanger 2 (HE2) is connected to the prosumer's distribution system directly and acts as a high-temperature heat source. It boosts the supply temperature of the prosumer to the required level after the preheating by low-temperature DHSs.

Moreover, the WTTES in the system is a short-term TES. As described in Section 1, it has two key functions. Firstly, it relives the mismatch problem between the DHS's heat supply and the buildings' heat demand during the warm period. When the DHS's heat supply is higher than the buildings' heat demand, the surplus heat supply from the DHS is stored in the WTTES instead of being fed into the central DH system. When the DHS's heat supply is lower than the buildings' heat demand, the stored heat in the WTTES together with the heat from DHS is supplied to the buildings. Secondly, the WTTES shaves the prosumer's peak load during the cold period. The WTTES is charged at non-peak hours and discharged at peak hours, therefore part of the central DH system's heat supply is shifted to non-peak hours and the peak load is shaved.

Finally, the heat-users in the system are buildings. As illustrated in Fig. 1, the heat-user may be one building when the prosumer is an individual prosumer or a cluster of buildings when the prosumer is a community prosumer.

### 2.3. Optimal operation for a prosumer with WTTES

To optimize prosumers' economic performance, the optimal operation strategy should minimize prosumers' heat use from the central DH system by increasing the self-utilization rate of the heat supply from prosumer's DHSs, minimize the prosumers' peak load. In addition, the operation should track the reference indoor temperature by minimizing the deviation between the simulated indoor temperature and its reference value. To achieve the above

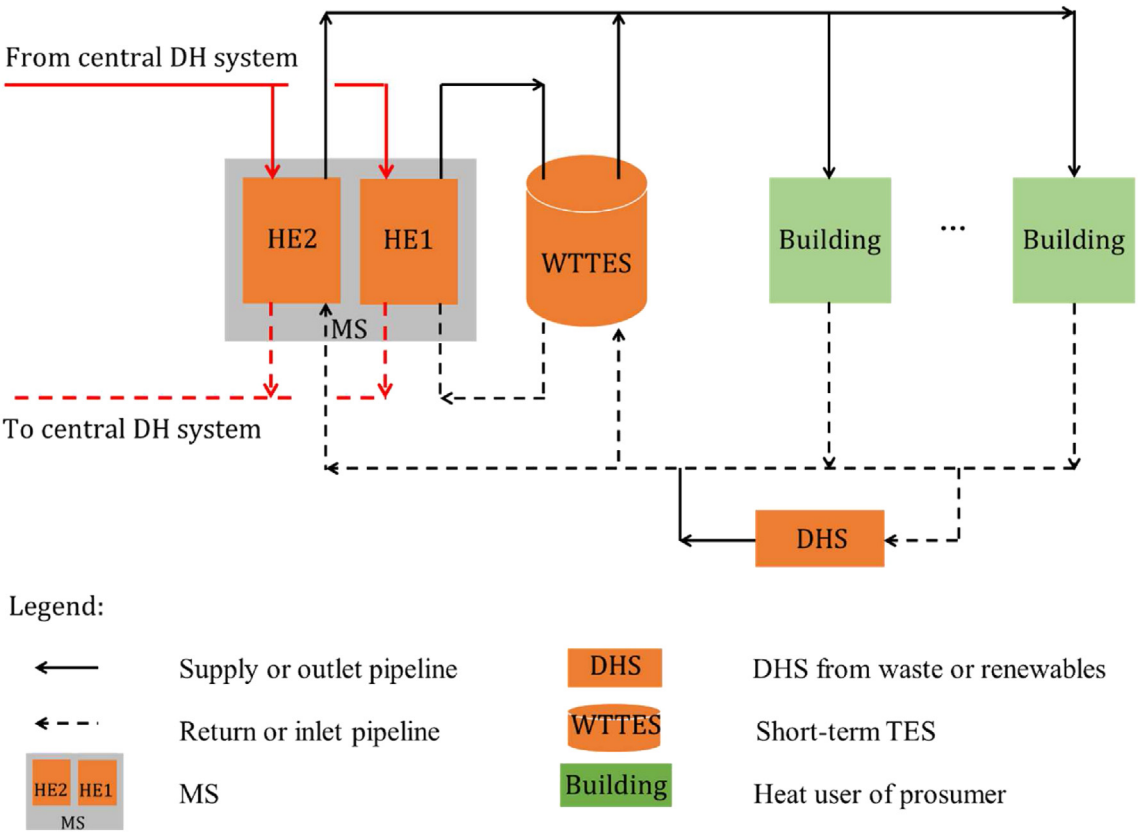


**Fig. 3.** Schematic illustrates the system design for a prosumer with WTTES.

goals, a multi-objective dynamic optimization problem was formulated as Equations (4), (5), (6), (7), and (8):

Minimize:

$$\int_{t_0}^{t_f} EP(t)\cdot\dot{Q}(t)dt + LP\cdot\dot{Q}_{pea} + W\cdot\int_{t_0}^{t_f}\left(T_{ia}(t) - T_{ia}^{ref}(t)\right)^2\cdot dt \tag{4}$$

subject to:

$$\dot{Q}(t) \le \dot{Q}_{pea} \tag{5}$$

$$F(t, \boldsymbol{z}(t)) = 0 \tag{6}$$

$$F_0(t_0, \boldsymbol{z}(t_0)) = 0 \tag{7}$$

$$z_L \le \boldsymbol{z}(t) \le z_U \tag{8}$$

where $\dot{Q}(t)$ is the heat flow rate supplied from the central DH to the prosumer. $\dot{Q}_{pea}$ and $LP$ are the peak load and the LDC heating price, respectively. $EP(t)$ is the heating price for the EDC. $T_{ia}(t)$ and $T_{ia}^{ref}(t)$ are the simulated indoor temperature and its reference value at time t. $\boldsymbol{z}\in\mathbb{R}^{n_z}$ represents the time-dependent variables, which includes the manipulated variable $\boldsymbol{u}\in\mathbb{R}^{n_u}$ to be optimized, the differential variable $\boldsymbol{x}\in\mathbb{R}^{n_x}$, and the algebraic variable $\boldsymbol{y}\in\ \mathbb{R}^{n_y}$. Equation (6) defines the system dynamics and Equation (7) is the initial conditions of the system. $z_L\in[-\infty,\infty]^{n_z}$ and $z_U\in\ [-\infty,\infty]^{n_z}$ are the lower and upper bounds, respectively.

The system dynamics defined in Equation (6) included the dynamics of the MS, TES, DHS, buildings, and pipelines, as illustrated in Fig. 3. The energy and mass flow exchanged between these components were described by Equations (9), (10), (11), (12), and (13).

$$\dot{Q}(t) = \dot{Q}_{HE1} + \dot{Q}_{HE2} \tag{9}$$

$$\dot{Q}_{HE1} + \dot{Q}_{HE2} + \dot{Q}_{DHS} = \dot{Q}_{Bui} + \dot{Q}_{TES} + \dot{Q}_{loss,\ TES} + \dot{Q}_{loss,\ pip} \tag{10}$$

$$\dot{Q}_{HE1} = c\cdot\dot{m}_{HE1}\cdot\left(T_{HE1,sup} - T_{HE1,ret}\right) \tag{11}$$

$$\dot{Q}_{HE2} = c\cdot\dot{m}_{HE2}\cdot\left(T_{HE2,sup} - T_{HE2,ret}\right) \tag{12}$$

$$\dot{Q}_{DHS} = c\cdot\dot{m}_{DHS}\cdot\left(T_{DHS,sup} - T_{DHS,ret}\right) \tag{13}$$

where $\dot{m}_{HE1}$, $\dot{m}_{HE2}$, and $\dot{m}_{DHS}$ are the mass flow rate of HE1, HE2, and DHS, respectively. $\dot{Q}_{HE1}$, $\dot{Q}_{HE2}$, and $\dot{Q}_{DHS}$ are the heat flow rate of HE1, HE2, and DHS, respectively. $\dot{Q}_{TES}$ is the charging (positive values) and discharging (negative values) heat flow rate of WTTES. $\dot{Q}_{Bui}$ is the heat demand of buildings. $\dot{Q}_{loss,\ TES}$ and $\dot{Q}_{loss,\ pip}$ are the heat loss from WTTES and pipelines, respectively. $T_{HE1,sup}$, $T_{HE2,sup}$, and $T_{DHS,sup}$ are the supply water temperature of HE1, HE2, and DHS, respectively. $T_{HE1,ret}$, $T_{HE2,ret}$, and $T_{DHS,ret}$ are the return water temperature of HE1, HE2, and DHS, respectively. $c$ is the specific heat capacity of water.

In this study, the manipulated variables, $\boldsymbol{u}$ in Equations (6), are the supply water temperature of HEs in the MS ($T_{HE1,sup}$ and $T_{HE2,sup}$), the mass flow rate of HEs and buildings ($\dot{m}_{HE1}$, $\dot{m}_{HE2}$, and $\dot{m}_{Bui}$), and the heat supply flow rate from the radiator to the

building ($\dot{Q}_{rad}$). The heat flow rate of a prosumer, $\dot{Q}(t)$ in Equation (4), means the total heat flow rate of the two HEs in MS ($\dot{Q}_{HE1}$ and $\dot{Q}_{HE2}$) as shown in Equation (9). In addition, the variables $\dot{Q}_{TES}$, $\dot{Q}_{loss,\ TES}$, $\dot{Q}_{Bui}$, and $\dot{Q}_{loss,\ pip}$ are described in the models of WTTES, buildings, and pipelines, which are explained in Sections 2.3.1-2.3.3.

### 2.3.1. Model for short-term WTTES

WTTES was chosen as the TES in this research because it is easily applied [37,38] and economically reasonable [39] for DH systems. A one-dimensional WTTES model was used to describe the dynamics of the thermocline tank. The model can be represented as a single partial differential equation as Equation (14) [40]:

$$c \cdot \rho \cdot A_{XS} \cdot \frac{\partial T}{\partial t} = c \cdot (\dot{m}_{sou} - \dot{m}_{use}) \cdot \frac{\partial T}{\partial x} - U \cdot P \cdot (T(t,x) - T_{amb}) + \varepsilon \cdot A_{XS} \cdot \frac{\partial^2 T}{\partial x^2} \tag{14}$$

where $T$ is the water temperature in the tank. $x$ is the height of the tank. $t$ is the time. $\rho$ is the density of water. $A_{XS}$ and $P$ are the cross-sectional area and the perimeter of the tank, respectively. $\dot{m}_{sou}$ and $\dot{m}_{use}$ are the water mass flow rate from the heat source side and the user side, respectively. $T_{amb}$ is the ambient temperature. $U$ is the U-value of the tank wall. $\varepsilon$ is a parameter representing the combined heat transfer effect of water through diffusion, conduction, and mixing due to turbulent flow.

To solve Equation (14) by using numerical methods, spatial derivatives were approximated by discretizing the tank into $n$ nodes. Using the discretization scheme shown in Fig. 4 and computing energy balances on each node, Equation (14) was converted into a set of ordinary differential equations. The ordinary differential equation for the *ith* node is shown in Equation (15) [40]. Therefore, the heat loss and the heat flow rate of the *ith* node are obtained by Equations (16) and (17), and the total heat loss and heat flow rate of WTTES was calculated as Equations (18) and (19). In addition, the parameter $\varepsilon$ has two different types of values representing the situations without and with buoyant mixing effect. When the temperature of a node is lower than the node above it, $\varepsilon$ has lower values. Otherwise, the values become several orders of magnitude higher due to the buoyant mixing effect [40].

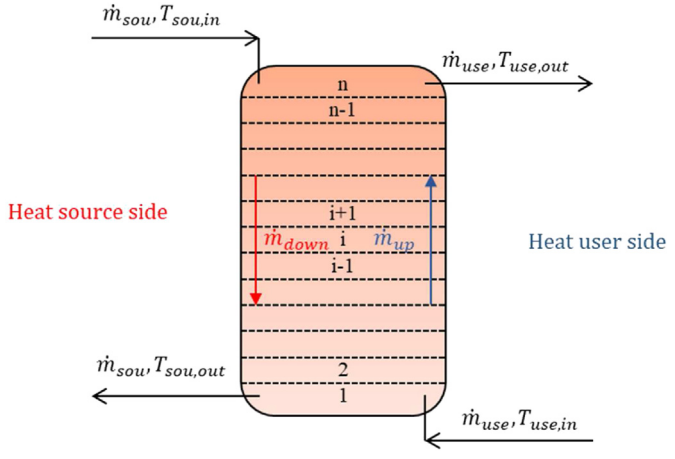


**Fig. 4.** Diagram illustrates the spatial discretization for a thermocline tank.

$$c \cdot \rho \cdot A_{XS} \cdot \Delta x \cdot \frac{dT_i}{dt} = c \cdot \dot{m}_{use} \cdot (T_{i-1} - T_i) + c \cdot \dot{m}_{sou} \cdot (T_{i+1} - T_i) - U \cdot P \cdot \Delta x \cdot (T_i - T_{amb}) + \frac{\varepsilon \cdot A_{XS}}{\Delta x} \cdot (T_{i+1} - 2 \cdot T_i + T_{i-1}) \tag{15}$$

$$\dot{q}_{loss,\ TES,\ i} = U \cdot P \cdot \Delta x \cdot (T_i - T_{amb}) \tag{16}$$

$$\dot{q}_{TES,i} = c \cdot \dot{m}_{sou} \cdot (T_{i+1} - T_i) \tag{17}$$

$$\dot{Q}_{loss,\ TES} = \sum_{i=1}^{n-1} \dot{q}_{loss,\ TES,\ i} \tag{18}$$

$$\dot{Q}_{TES} = \sum_{i=1}^{n-1} \dot{q}_{TES,i} \tag{19}$$

where $\Delta x$ is the length of the node, and $T_i$ is the water temperature of the *ith* node. $\dot{q}_{loss,\ TES,\ i}$ and $\dot{q}_{TES,i}$ are the heat loss and heat flow rate of the *ith* node, respectively.

### 2.3.2. Model for buildings

To improve computational efficiency, a single-equivalent building model was used to represent the overall performance of all the buildings in this study. This simplification has been proved feasibility by previous research [39,41]. After these simplifications, Equation (20) is used to describe the thermal behaviours of all the buildings connected to the prosumer' heating system, and Equations (21)–(23) are the inequality constraints for the variables $\Delta T_{Bui}$, $T_{sup}$, and $\dot{m}_{Bui}$.

$$\dot{Q}_{Bui} = c \cdot \dot{m}_{Bui} \cdot (T_{sup} - T_{ret}) \tag{20}$$

$$\Delta T_{Bui,\ L} \le \Delta T_{Bui} = T_{sup} - T_{ret} \le \Delta T_{Bui,U} \tag{21}$$

$$T_{sup,L} \le T_{sup} \le T_{sup,U} \tag{22}$$

$$\dot{m}_{Bui,\ L} \le \dot{m}_{Bui} \le \dot{m}_{Bui,\ U} \tag{23}$$

where $\dot{Q}_{Bui}$ is the buildings' heat demand including demand for the SH and the DHW system. $\dot{m}_{Bui}$ and $\Delta T_{Bui}$ are the mass flow rate and temperature difference of water at the primary side of the building's substation, respectively. $T_{sup}$ and $T_{ret}$ are the supply and return temperature of water at the primary side of the building's substation, respectively. $\Delta T_{Bui,\ L}$, $T_{sup,L}$, and $\dot{m}_{Bui,\ L}$ are the lower bounds for $\Delta T_{Bui}$, $T_{sup}$, and $\dot{m}_{Bui}$, respectively. $\Delta T_{Bui,U}$, $T_{sup,U}$, and $\dot{m}_{Bui,\ U}$ are the upper bounds for $\Delta T_{Bui}$, $T_{sup}$, and $\dot{m}_{Bui}$, respectively.

The lower bound of the supply temperature, $T_{sup,L}$, should be high enough for the SH system and the DHW system to keep a comfortable indoor temperature and avoid hygiene issues, as defined in Equation (24). The lower bound of the supply temperature was defined by Equation (25) for the SH system [42], and the lower bound of the supply temperature for the DHW system was 60 °C as defined in Equation (26), which is required by European standard CEN/TR16355 [43]. In addition, the upper bound for the supply temperature was determined by the supply temperature of

the central DH system, which can be deduced through measured data.

$$T_{sup,L} = max(T_{sup,SH,L}, T_{sup,\ DHW,L}) \tag{24}$$

$$\begin{aligned} T_{sup,SH,L} = {} & T_{ia} \\ & + 0.5 \cdot \left(T_{sup,SH,des} + T_{ret,SH,des} - 2 \cdot T_{ia,des}\right) \cdot \left(\frac{T_{ia,des} - T_{oa}}{T_{ia,des} - T_{oa,des}}\right)^{1/b} \\ & + 0.5 \cdot \left(T_{sup,SH,des} - T_{ret,SH,des}\right) \cdot \left(\frac{T_{ia,des} - T_{oa}}{T_{ia,des} - T_{oa,des}}\right) \end{aligned} \tag{25}$$

$$T_{sup,\ DHW,L} = 60 \tag{26}$$

where $T_{sup,SH,L}$ and $T_{sup,\ DHW,L}$ are the lower bound of the supply temperature for the SH and the DHW system, respectively. $T_{ia}$ and $T_{oa}$ are the indoor and the outdoor temperature, respectively. $T_{sup,SH}$ and $T_{ret,SH}$ are the supply and the return temperature of the SH system, respectively. $b$ is a parameter depending on the characteristic of the radiator. The subscript *des* refers to the design conditions.

The lower bound of the water mass flow rate $\dot{m}_{Bui,L}$ is zero, and the upper bound of the water mass flow rate $\dot{m}_{Bui,U}$ is constrained by the capacity of the distribution system. In this study, the upper bound of the water mass flow rate $\dot{m}_{Bui,U}$ was obtained by the measurement data. In addition, the characteristics of the system and equipment determine the feasible region of the water temperature difference as described in Equation (21). In this study, the lower bound of the water temperature difference $\Delta T_{Bui,\ L}$ was zero, and the upper bound of the water temperature difference $\Delta T_{Bui,U}$ was obtained by the linear regression using measured data as Equation (27).

$$\Delta T_{Bui,U} = a_0 + a_1 \cdot T_{sup} \tag{27}$$

where $a_0$ and $a_1$ are parameters.

The buildings' heat demand, $\dot{Q}_{Bui}$, includes the heat demand for the SH and the DHW system, as in Equation (28).

$$\dot{Q}_{Bui} = \dot{Q}_{SH} + \dot{Q}_{DHW} \tag{28}$$

where $\dot{Q}_{SH}$ and $\dot{Q}_{DHW}$ are the heat demand of the SH and the DHW systems, respectively. $\dot{Q}_{SH}$ can be further divided into the demand for the radiator heating system $\dot{Q}_{rad}$ and the demand for the ventilation system $\dot{Q}_{ven}$, as described in Equation (29).

$$\dot{Q}_{SH} = \dot{Q}_{rad} + \dot{Q}_{ven} \tag{29}$$

Considering the thermal inertia of buildings, a simplified-lumped-capacity model derived from resistance-capacitance networks analogue to electric circuits was used to describe the building dynamics, as defined in Equations (30)–(32).

$$C_{env} \cdot \frac{dT_{env}}{dt} = \frac{T_{ia} - T_{env}}{R_{i,e}} + \frac{T_{oa} - T_{env}}{R_{o,e}} \tag{30}$$

$$\begin{aligned} C_{ia} \cdot \frac{dT_{ia}}{dt} = {} & \frac{T_{ma} - T_{ia}}{R_{i,m}} + \frac{T_{env} - T_{ia}}{R_{i,e}} + \frac{T_{oa} - T_{ia}}{R_{win}} + \frac{T_{oa} - T_{ia}}{R_{ven}} + \dot{Q}_{rad} \\ & + \dot{Q}_{ven} + \dot{Q}_{in} \end{aligned} \tag{31}$$

$$C_{ma} \cdot \frac{dT_{ma}}{dt} = \frac{T_{ia} - T_{ma}}{R_{i,m}} \tag{32}$$

where $C$ and $R$ represent the heat capacitance and resistance, $T$ is the temperature. Subscripts *env*, *ia*, *oa*, *ma*, *win*, and *ven* denote building envelopes (including exterior walls and roofs), indoor air, outdoor air, internal thermal mass, window, and ventilation (including infiltration and mechanical ventilation), respectively. In addition, $R_{i,e}$ is the heat resistance between the indoor air and the building envelopes, $R_{o,e}$ is the heat resistance between the outdoor air and the building envelopes, and $R_{i,m}$ is the heat resistance between indoor air and interior thermal mass. $\dot{Q}_{in}$ is the internal heat gains. All the introduced heat capacitances, thermal resistances, temperatures, and heat flow rates in Equations (30)–(32) are marked in Fig. 5.

### 2.3.3. Model for pipelines

The pipeline model representing the heat loss from the pipelines was described as the following Equations (33)–(35) [44]:

$$\dot{Q}_{loss,\ pip} = \dot{Q}_{loss,\ pip,sup} + \dot{Q}_{loss,\ pip,ret} \tag{33}$$

$$\dot{Q}_{loss,\ pip,sup} = L \cdot \pi \cdot d \cdot \frac{(R_g + R_i) \cdot \Delta T_{pip,sup} - R_c \cdot \Delta T_{pip,ret}}{(R_g + R_i)^2 - R_c^2} \tag{34}$$

$$\dot{Q}_{loss,\ pip,ret} = L \cdot \pi \cdot d \cdot \frac{(R_g + R_i) \cdot \Delta T_{pip,ret} - R_c \cdot \Delta T_{pip,sup}}{(R_g + R_i)^2 - R_c^2} \tag{35}$$

where $\dot{Q}_{loss,\ pip}$, $\dot{Q}_{loss,\ pip,sup}$, and $\dot{Q}_{loss,\ pip,ret}$ are the total heat loss from pipes, the heat loss from supply pipes, and the heat loss from return pipes, respectively. $L$ is the route length for the pair of pipes. $d$ is the outer pipe diameter. $R_i$, $R_g$, and $R_c$ are the resistances for insulation, ground, and coinciding, respectively, and they can be obtained by Equations (36)–(38). In addition, $\Delta T_{pip,sup}$ and $\Delta T_{pip,ret}$ are the temperature difference for the supply pipe and the return pipe, and can be obtained by Equations (39) and (40):

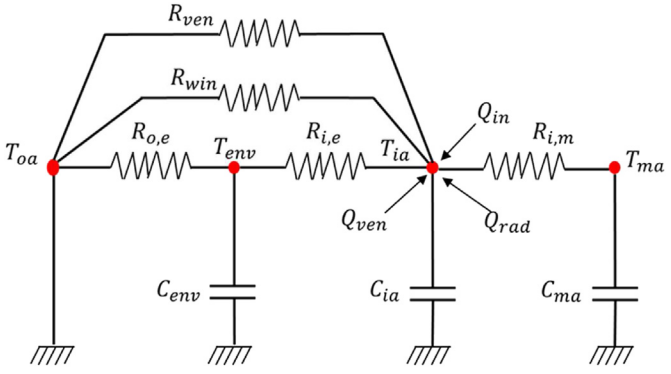


**Fig. 5.** Schematic of the simplified-lumped-capacity building model.

$$R_i = \frac{d}{2 \cdot \lambda_i} \cdot ln \frac{D}{d} \tag{36}$$

$$R_g = \frac{d}{2 \cdot \lambda} \cdot ln \frac{4 \cdot h}{D} \tag{37}$$

$$R_c = \frac{d}{2 \cdot \lambda} \cdot ln \left( \frac{2 \cdot h}{s} \right) \left( \frac{2 \cdot h}{s} \right) \left( \left( \frac{2 \cdot h}{s} \right)^2 + 1 \right)^{0.5} \tag{38}$$

$$\Delta T_{pip,sup} = T_{pip,sup} - T_{grou} \tag{39}$$

$$\Delta T_{pip,ret} = T_{pip,ret} - T_{grou} \tag{40}$$

where $D$ is the outer insulation diameter, $h$ is the distance between the pipe centres and the ground surface, $s$ is the distance between pipe centres, and $\lambda$ and $\lambda_i$ are the heat conductivity for the ground and insulation. In addition, $T_{grou}$ is the ground temperature, which was obtained from Equations (41)–(43). $T_{pip,sup}$ and $T_{pip,ret}$ are the water temperature in the supply pipe and the return pipe, respectively.

### 2.3.4. Model for the ground

In this study, the WTTES model and pipelines model used the ground temperature to calculate the heat losses. Equations (41)–(43) were applied to estimate the ground temperature as follows [45]:

$$T_{grou}(z,t) = T_{oa,aver} - T_{peak} \cdot e^{-z \cdot \sqrt{\frac{\omega}{2 \cdot \alpha}}} \cdot cos\left( \omega \cdot t - \phi - z \cdot \sqrt{\frac{\omega}{2 \cdot \alpha}} \right) \tag{41}$$

$$\omega = \frac{2 \cdot \pi}{T_{peri}} \tag{42}$$

$$\alpha = \frac{k}{\rho \cdot C} \tag{43}$$

where $T_{grou}(z,t)$ is the ground temperature in the depth $z$ and at time $t$. $T_{oa,aver}$ is the annual average temperature of the outdoor air. $T_{peak}$ is the peak deviation of the function from zero. $\omega$ is the angular frequency, $T_{peri}$ is the period of the temperature cycle, and $\phi$ is the phase. $\alpha$, $k$, $\rho$, and $C$ are the thermal diffusivity, thermal conductivity, density, and heat capacity of the ground, respectively.

### 2.4. Indicators to evaluate the economic performance

In this section, the economic indicators including the initial investment cost and the payback period are introduced to evaluate the economic performance of the heat prosumers with TESs. The initial investment cost required for the WTTES depends strongly on the storage size. Fig. 6 illustrates the relationship between the initial investment cost and the size of WTTESs that with storage volumes larger than 200 m$^3$. The black dots in Fig. 6 present previous projects [52]. Fig. 6 shows that a power function approximates the relationship very well, with a coefficient of determination ($R^2$) of 0.99 and without obvious overfitting. In this study, the power function in Equation (44) was used to estimate the initial investment cost for large scale WTTESs in DH systems.

$$Invt = 0.0047 \cdot V^{0.6218} \tag{44}$$

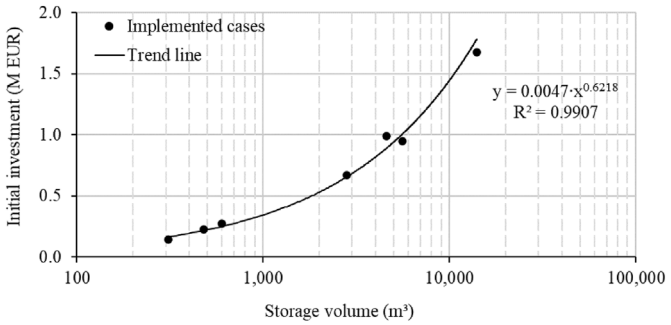


**Fig. 6.** The initial investment cost for WTTES.

where $Invt$ is the initial investment cost and $V$ is the storage volume of WTTES.

The payback period is the time taken to fully recover the initial investment cost. It is one of the most commonly used methods for evaluating the economic performance of a system [47]. The payback period, $PB$, was calculated by using Equation (45):

$$B_{sav} \cdot \frac{(1+i)^{PB} - 1}{i \cdot (1+i)^{PB}} - Invt = 0 \tag{45}$$

where $B_{sav}$ is the annual energy bill saving and $i$ is the prevailing interest rate.

## 3. Case study

The proposed method in Section 2 was tested on a campus DH system in Norway. The background of the case study, research scenarios, and simulation settings are introduced below.

### 3.1. Background for the case study

A campus DH system in Trondheim, Norway, was chosen as the case study. As illustrated in Fig. 7, the campus DH system is a prosumer with DHS and heat users. The DHS is the university DC, which recovers the condensing waste heat from its cooling system. The heat users are buildings at the campus with a total building area of 300,000 m$^2$. The campus DH system is connected to the central DH system via the MS. Detailed information on the campus DH system can be found in Refs. [48,49]. According to the measurements from June 2017 to May 2018, the total heat supply for the campus DH system was 32.8 GWh. About 80% of the heat supply comes from the central DH system through the MS. The other 20% comes from the waste heat recovery from the DC.

Fig. 8 plots the heat demand for buildings and waste heat from the DC for the year 2017–2018. As shown with the green line in Fig. 8, the waste heat supply from the DC was around 1.0 MW throughout the year. However, as shown with the black line in Fig. 8, the building heat demand fluctuated from 0.2 MW to 13.8 MW. The mismatch between the waste heat supply and the building heat demand resulted in the surplus waste heat supply, especially for the period between June to October, as shown with the red line of Fig. 8. This surplus waste heat supply was fed into the central DH system via the MS. However, the university got no economic benefit from this surplus waste heat fed in, because as introduced in Section 1, the current heating price models do not support the reverse heat supply from the end-users to the central DH system.

In addition, the building heat demand was not equally distributed and there were high peak loads during the period from

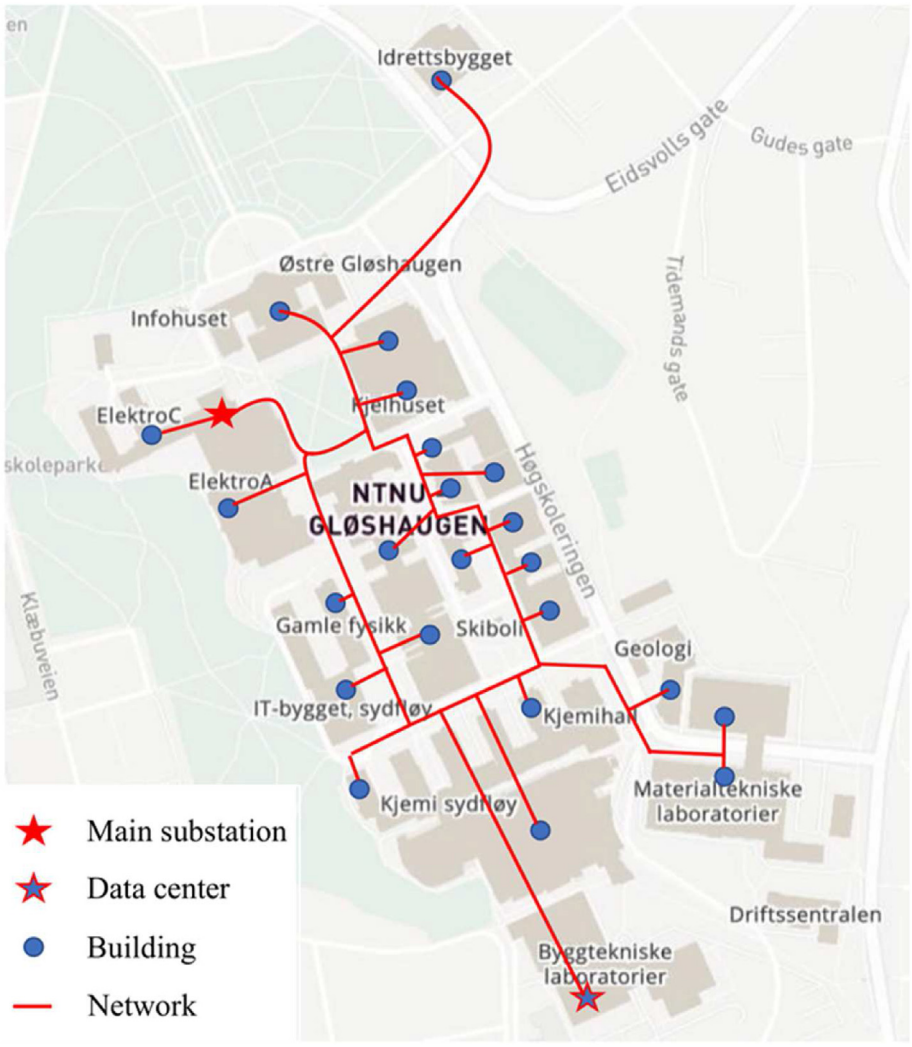


**Fig. 7.** Campus district heating system.

November to March, as shown with the black line of Fig. 8. The local DH company charged the heating bill also considering the peak load and the university paid about 5.3 million NOK[1] for the peak load each year, which accounted for 26% of the total heating bill.

### 3.2. Scenarios and simulation settings

To explore the economic feasibility after introducing a WTTES to the prosumer, different research scenarios were proposed based on the storage capacity of WTTES. The storage capacity meant the maximum discharging time for a WTTES under the discharging heat flow rate equals buildings' annual average heat demand. Eight scenarios including the reference scenario were proposed as listed in Table 1. The reference scenario, *Ref*, represented the current campus DH system without any TES. The other scenarios represented the WTTES solutions with storage capacities ranging from three hours to one week. The WTTESs were cylinder-shaped. All the tanks had the same height of 15 m, while the diameters were modified to provide certain storage capacities.

This research was conducted through three steps. Firstly, WTTESs with different storage capacities were integrated into the prosumer's campus DH system, respectively, as introduced in Section 2.2. Secondly, the optimal operation trajectories for the prosumer's campus DH system with the different storage capacities were obtained through the method provided in Section 2.3. Finally, these operation trajectories were evaluated in terms of economic indicators explained in Section 2.4. This study was based on the conditions of the year 2017–2018, and the detailed settings for the simulations are explained as follows. The used buildings' heat demand and the DC's waste heat came from the measured data as shown in Fig. 8. The key parameter settings are presented in Table A 1 in Appendix A. Among them, the parameters for the WTTES model were set according to the research [50], and the parameters of the pipeline model were set based on the book [44]. In addition, the heating prices were obtained from the website of the local DH company [51]. The local DH company used the monthly EDC heating price as shown in Fig. A 1 in Appendix A. Meanwhile, the used LDC heating price was 33 NOK/kW/month. Measured air temperature and estimated ground temperature of the simulation year are presented in Fig. A 2 in Appendix A.

## 4. Results

This section firstly presents the model validation results and

[1] The currency rate between NOK and EUR can be found from https://www.xe.com/, in this study 1 EUR = 10 NOK.

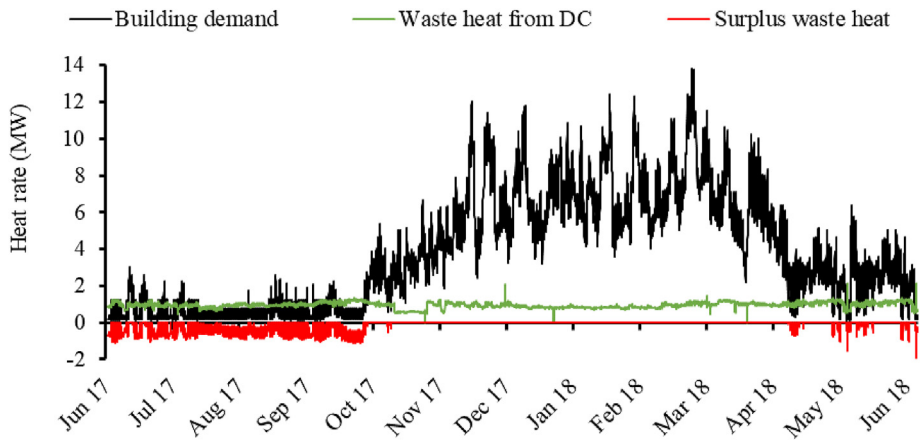


**Fig. 8.** Heat demand and waste heat supply.

**Table 1**
Information for the scenarios.

| Scenario abbreviation | Storage capacity (hour) | Storage volume ($m^3$) | Tank diameter (m) |
|---|---|---|---|
| Ref | N/A | N/A | N/A |
| 3 h | 3 | 200 | 4.1 |
| 6 h | 6 | 400 | 5.8 |
| 12 h | 12 | 900 | 8.7 |
| 1 d | 24 | 1700 | 12.0 |
| 3 d | 72 | 5200 | 21.0 |
| 5 d | 120 | 8600 | 27.0 |
| 7 d | 168 | 12,000 | 31.9 |

then evaluates the proposed scenarios in terms of energy and economic analyses.

### 4.1. Model validation

As introduced in Section 2.3, the system model includes the following components: the WTTES, the building, and pipelines. In this study, the current campus DH system does not have any WTTES, and there is no measured data for the heat loss from the pipelines as well. Therefore, the WTTES and the pipeline model were validated according to the reference values from technical reports and textbooks instead of measured data. In a report from the International Energy Agency on large scale TESs [52], the reference storage efficiency for a WTTES is 50–90%. In this study, the corresponding value was about 90%, which was within the reference range. In practice, the low storage efficiency is caused by moistened insulation, because these WTTESs' envelopes are often deficient to protect against moisture penetration. However, it was assumed that the WTTES's envelope had a good quality to protect moisture penetration. Therefore, the WTTES used in this research had high storage efficiency.

According to the textbook *District Heating and Cooling* [44], for the DH systems in high heat density areas, the reference values for pipeline heat loss is 5–8% of the total heat supply. In this study, the corresponding value was close to 5%. This low pipeline heat loss was caused by two reasons. Firstly, compared to the typical DH systems with linear heat densities lower than 20 MWh/(m·a), the studied campus DH system had a higher linear heat density of 22 MWh/(m·a). The higher linear heat density made it more efficient during the distribution process and hence led to less pipeline heat loss. Secondly, the studied campus DH system had an annual average supply temperature of 65 °C that was lower than the typical DH system with 70–80 °C. Therefore, the low-temperature difference between the pipelines and the ground led to low pipeline heat loss.

The building model proposed in Section 2.3.2 was validated against the measured data. To quantify the deviation of the simulated data from the measured data, two indicators, i.e. coefficient of variation of the root mean square error (CV(RMSE)) and normalized mean bias error (NMBE), were used to evaluate the prediction performance of building model according to ASHRAE Guideline 14–2014 [53]. The validation criteria required in ASHRAE Guideline 14–2014 is within ±30% for CV(RMSE) and within ±10% for NMBE when using hourly data [53]. Fig. 9 shows the hourly simulated and measured building heat demand. As shown in Fig. 9, the values of the two indicators satisfied the requirements. In addition, Fig. 9 shows that the simulated building heat demand captured the trend in the measured data very well, with coefficients of determination ($R^2$) higher than 0.9 and no obvious overfitting.

### 4.2. Peak load shaving and heat use saving

The heat load duration diagram for the proposed scenarios is illustrated in Fig. 10, and the corresponding peak load is presented in Fig. 11. As shown in Fig. 10, compared to the reference scenario, *Ref*, part of the heat load for the scenarios with WTTES was shifted from the peak hours (the area highlighted with red colour) to the non-peak hours (the area highlighted with green colour). This load shifting contributed to the peak load shaving effect. As shown in Fig. 11, all the scenarios with WTTES had a lower peak load compared to the reference scenario. Furthermore, the load shifting effect was more significant for the scenarios with the larger WTTES. The maximal peak load shaving effect was achieved by scenario *7 d*, which had the largest WTTES. The peak load was shaved from 10.8 MW to 6.6 MW, a reduction of 39%. In contrast, the scenario with the smallest WTTES, *3 h*, had minimal peak load shaving, a reduction of only 4%.

Fig. 12 presents the annual heat use for the proposed scenarios. As introduced in Section 2.3, the prosumer's heat use means the heat supply from the central DH system via the MS. As shown in Fig. 12, the scenarios with the medium size WTTES (*3h*, *6 h*, *12 h*, and *1 d*) had minimal heat use, about 26.1 GWh, a heat use saving of 0.4 GWh compared to the reference scenario, *Ref*. However, the scenarios with the larger WTTES (*3 d*, *5 d* and *7 d*) had more heat use and hence less heat use saving. These results may be explained by Fig. 13. As shown by the columns filled with the orange colour in Fig. 13, the larger WTTES showed better performance on the

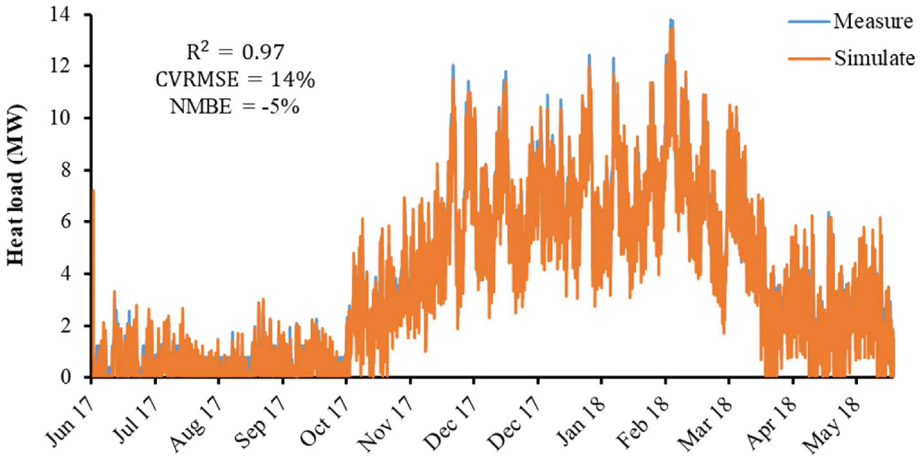


**Fig. 9.** Comparison between the simulated and measured building heat demand.

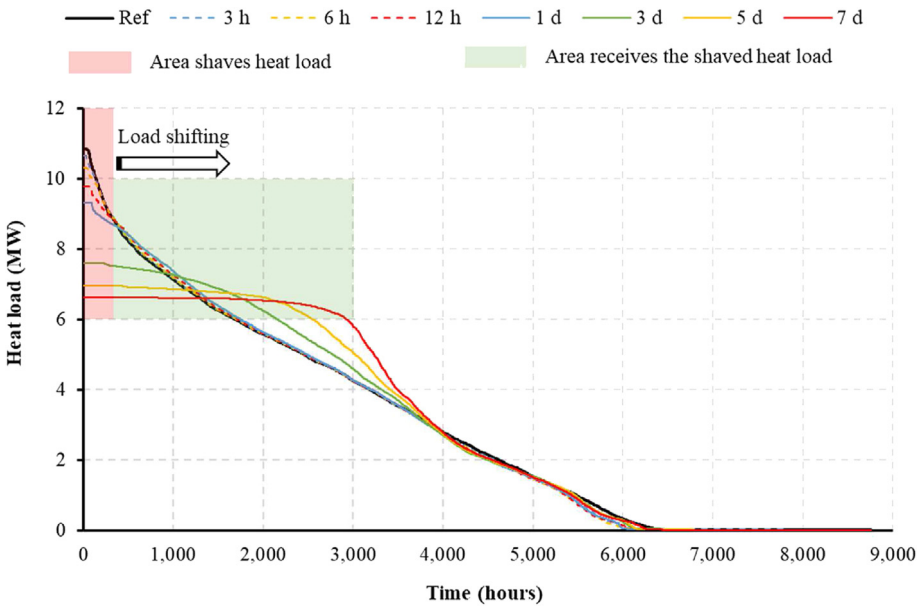


**Fig. 10.** Heat load duration diagram for the proposed scenarios.

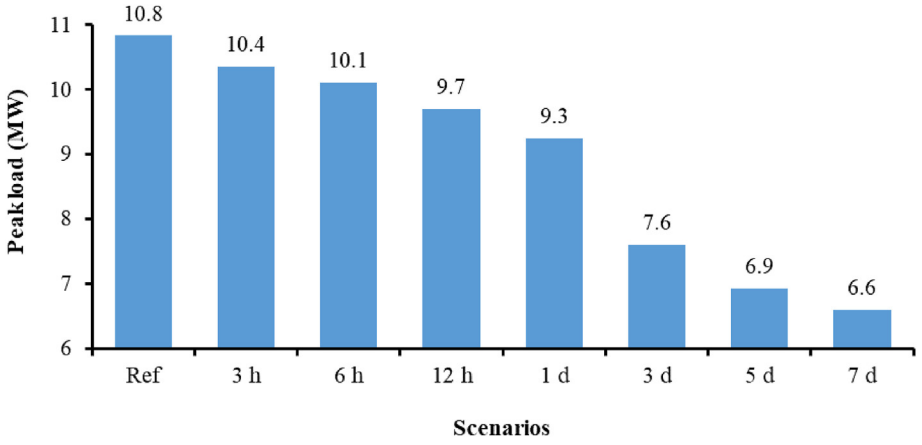


**Fig. 11.** Peak load for the proposed scenarios.

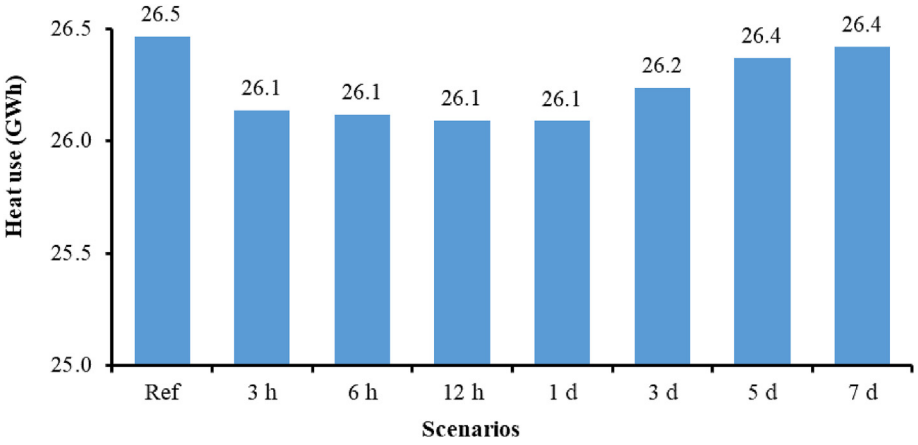


**Fig. 12.** Annual heat use for the proposed scenarios.

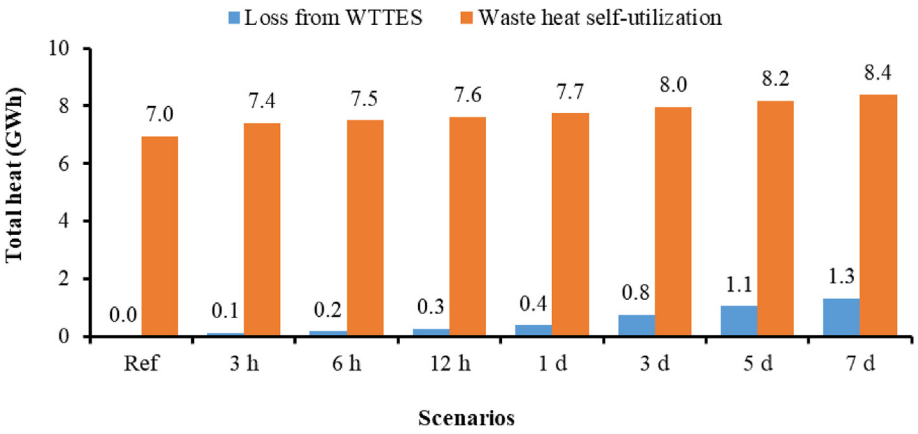


**Fig. 13.** Annual WTTES's heat loss and DC's waste heat self-utilization for the proposed scenarios.

mismatch relieving, and the waste heat self-utilization rate was increased from 79% to 96% (7.0 GWh to 8.4 GWh). However, the larger WTTES had higher heat loss to the environment as the columns filled with the blue colour in Fig. 13, because of its larger heat transfer area. The overall heat use saving performance of the WTTES depended on the sum of the above two effects. For the smaller WTTES, the mismatch relieving effect dominated the overall heat use performance. In contrast, for the larger WTTES, the heat loss effect dominated the overall heat use performance. Consequently, in this study, the WTTESs with three hours' to one day's storage capacity were the optimized storage size in terms of heat use saving.

### 4.3. Heating cost saving and payback period

The annual heating cost for the proposed scenarios is presented in Fig. 14 and the corresponding heating cost saving is shown in Fig. 15. Please note that all the currency in this section is presented in NOK. Two phenomena could be observed through Figs. 14 and 15: 1) the heating cost saving mainly came from the LDC, and 2) the larger WTTES brought more significant heating cost saving. As shown in Fig. 14, the annual EDC heating cost for the proposed scenarios was 15.4±0.1 million NOK, and the difference among these scenarios was less than 1%. In contrast, the annual LDC heating cost ranged from 4.7 million NOK to 2.8 million NOK with the increasing storage capacity of the WTTES, meaning a maximum difference of 39%. This significant reduction in the LDC contributed to the total heating cost saving. As shown in Fig. 15, as increasing the storage capacity of the WTTES, the annual heating cost saving increased from 0.4 million NOK to 1.9 million NOK, meaning a saving of 2%–9%. In this study, despite the waste heat self-utilization rate was increased up to 96%, as explained in Section 4.2, the relieving mismatch problem played a limited role in heating cost saving due to the original high waste heat self-utilization rate of 79%. However, for other cases with lower waste heat self-utilization rates, the relieving mismatch problem may contribute more to heating cost savings.

Fig. 16 presents the payback periods for the scenarios with the WTTES. It can be seen that the payback periods ranged from four years to ten years with the increasing WTTES storage size. Although the scenario with the largest WTTES needed the longest payback period, it achieved the highest heating cost saving. In contrast, the scenario with the smallest WTTES saved the lowest heating cost, while its payback period was the shortest. Therefore, the prosumer should make a trade-off between the payback period and the heating cost saving based on its own economic situation.

## 5. Discussion

This section first discusses the impacts of peak load definition on prosumers' economic performance. Afterwards, the thermoclines of the WTTESs during the charging and discharging processes are investigated.

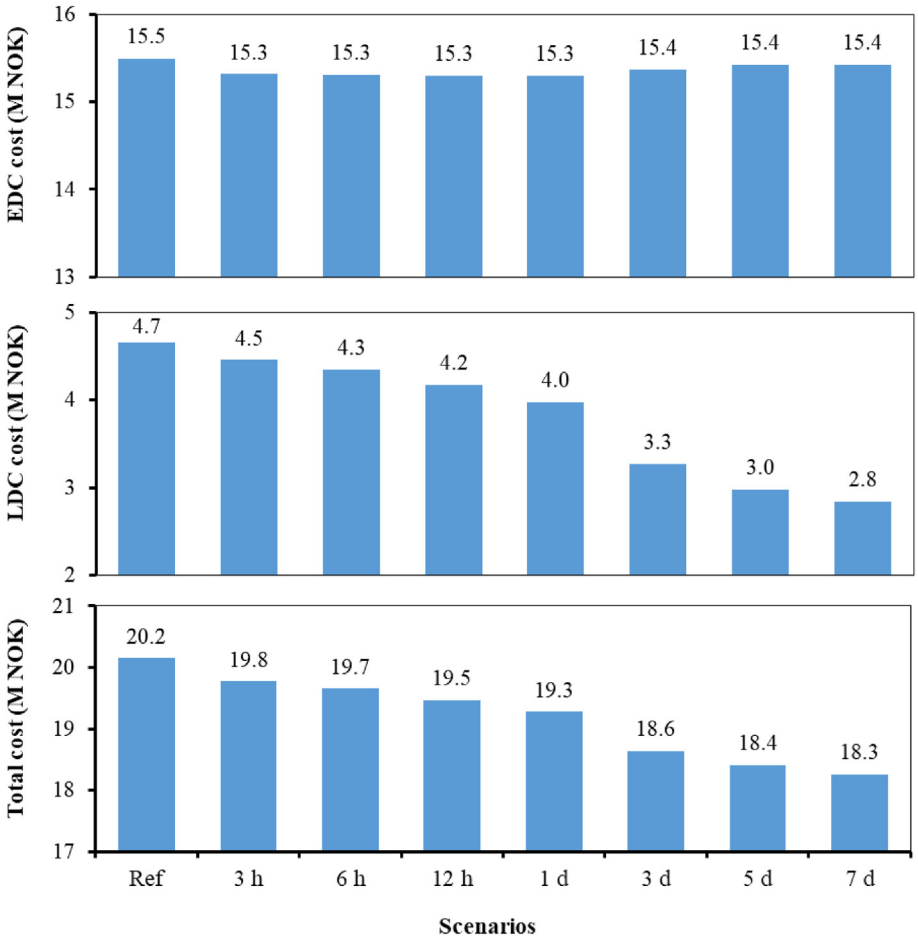


**Fig. 14.** Annual heating cost for the proposed scenarios.

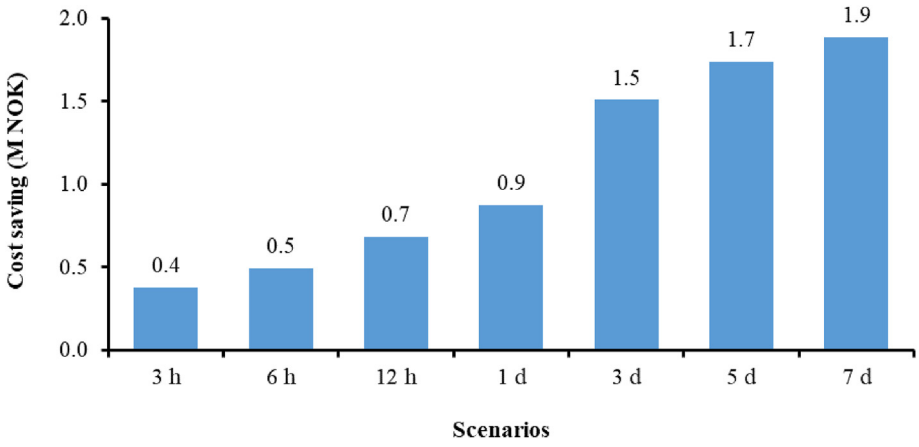


**Fig. 15.** Annual heating cost saving for the proposed scenarios.

### 5.1. Impacts of peak load definition

Based on a survey of heating contracts, methods of defining the peak load may be divided into two categories: hourly method and daily method [54]. For the hourly method, the peak load was the maximum hourly heat use, while the daily method was the maximum daily heat use. For this case study, the total heating cost saving was mainly determined by the reduction in LDC as observed in Section 4.3, which was linked to the peak load. Therefore, the way of defining the peak load may have a significant impact on the economic performance of prosumers with WTTESs. The results presented in Section 4 are based on the hourly method and this section presents further results based on the daily method.

The peak load under the daily method for the proposed scenarios is illustrated in Fig. 17, and the corresponding heating cost saving and the payback period are presented in Fig. 18 and Fig. 19,

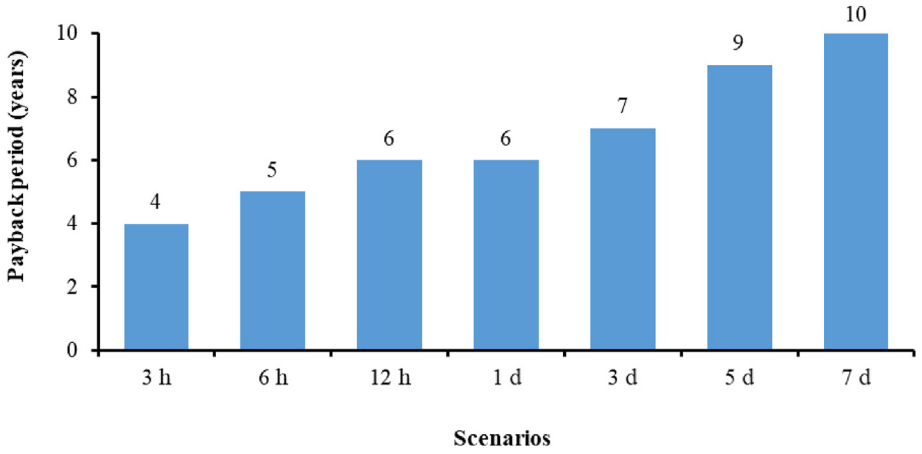


**Fig. 16.** The payback period for the scenarios with WTTES.

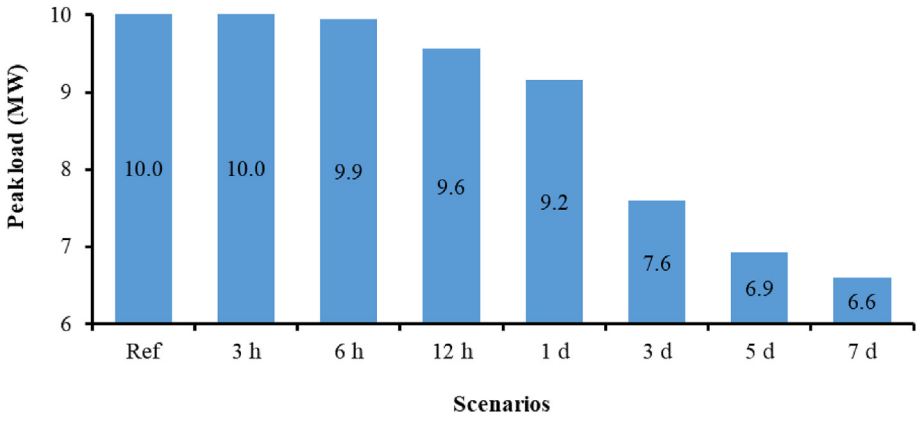


**Fig. 17.** Peak load for the proposed scenarios under the daily method.

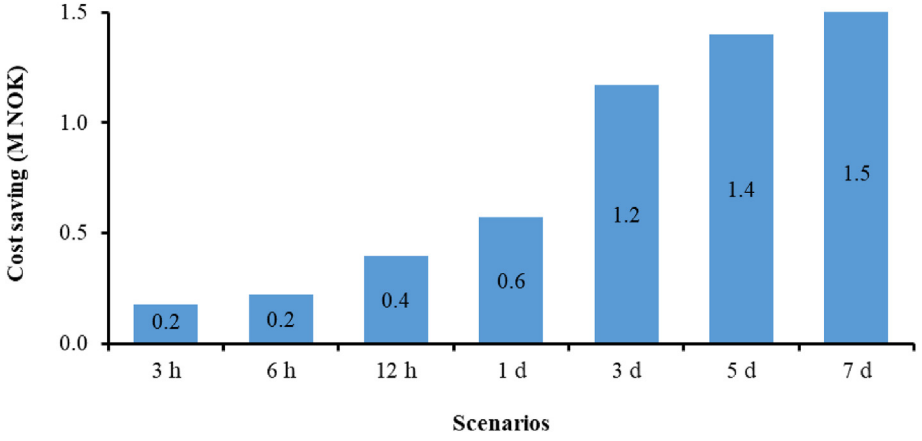


**Fig. 18.** Heating cost saving for the proposed scenarios under the daily method.

respectively. Similar to the hourly method, the larger WTTES brought a higher peak load shaving effect under the daily method as presented in Fig. 17. The peak load shaving increased from 0.1 MW to 3.4 MW as the increasing storage capacity of the WTTES from six hours to one week. However, compared to the hourly method, the peak load shaving effect under the daily method was different in two aspects: 1) it was less significant, and 2) it was not observed for the scenarios with the small WTTES. As shown in Fig. 17, the maximal peak load shaving effect was 3.4 MW, which was 19% less compared to the hourly method. Moreover, no peak load shaving effect was observed for the scenarios with the storage capacity smaller than six hours, their peak loads equalled that of the reference scenario, *Ref*, with the same value of 10.0 MW. The smaller WTTESs had a limited peak load shifting effect and was only capable to shift the heat load at the hourly level instead of the daily level. Therefore, the daily heat load kept almost the same.

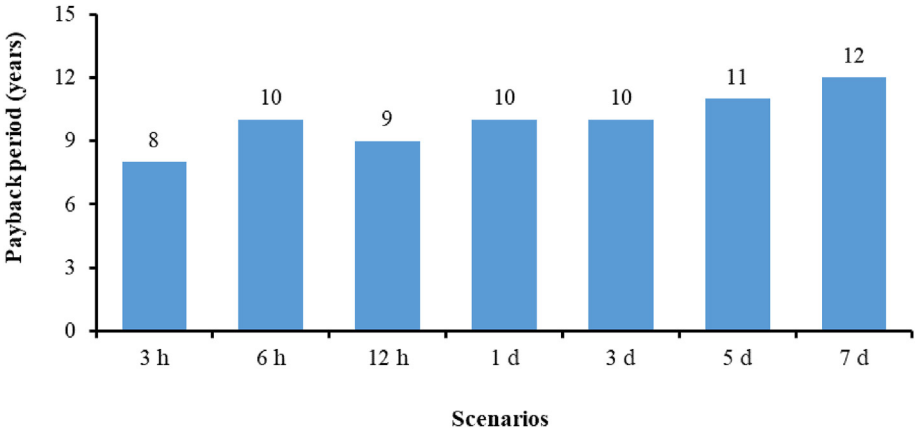


**Fig. 19.** The payback period for the proposed scenarios under the daily method.

The above impacts on the peak load shaving led to further impacts on the prosumer's economic performance. The prosumer obtained less heating cost saving under the daily method. As shown in Fig. 18, the heating cost saving ranged from 0.2 million NOK to 1.5 million NOK under the daily method, which was 18%–54% less compared to the hourly method. Furthermore, the payback period under the daily method ranged from 8 years to 12 years, and it was longer than the hourly method, especially for the WTTESs with smaller storage volumes.

Some recommendations from the discussion on the peak load definition are given as follows. Firstly, for the heat prosumers, special attention should be paid to the effect of the peak load definition. It may bring economic risk due to the changing of the heating contract. For example, DH companies may change their methods of defining the peak load from the hourly method to the daily method, and hence the economic benefit on heating cost saving may be drastically reduced and the payback period for TESs may be significantly prolonged. Secondly, for DH companies, it is better to use the hourly method to define the peak load, because the heat prosumers would be more motivated to introduce TESs and participate in user-side heat load management. One vital advantage brought by the user-side heat load management is peak load shaving, which may bring significant economic and technical benefits for DH companies.

### 5.2. Thermocline of the WTTES

In a WTTES, a thermocline is a layer where the water temperature changes more dramatically with depth than in the layers above and below it. It separates the lower density hot water at the top of the tank from the higher density cold water at the bottom of the tank. Generally, the thermocline should be as thin as possible to obtain a better thermal stratification and a less mixing effect between the hot and cold water [55]. Moreover, the position of the thermocline should be adjusted as the result of the optimized charging and discharging processes. Research showed that an optimal thermocline condition guaranteed high performance of the WTTES. For example, according to a study, the storage efficiency may be improved by 6% by optimizing the charging and discharging processes that led to an optimal thermocline condition [56]. Similar results were obtained in this study, which highlighted the importance of the thermocline of the WTTES. To assist the analysis of thermocline, the variable dimensionless temperature was used. As calculated by Equation (46), the water temperature of an individual layer in the WTTES was scaled into a real number ranging from 0 to 1. The two extreme values, 0 and 1, indicated the lowest and highest water temperature among all the layers in the WTTES. In a figure that illustrates the distribution of dimensionless temperature of layers in a WTTES, the thermocline can be identified as the layer that has significantly higher dimensionless temperature gaps between the layers above and below it.

$$T_{i,nonD} = \frac{T_i - T_{i,min}}{T_{i,max} - T_{i,min}} \tag{46}$$

where $T_{i,nonD}$ is the dimensionless water temperature of the Layer $i$. $T_i$ is the water temperature of the Layer $i$. $T_{i,max}$ and $T_{i,min}$ are the highest and lowest water temperatures among all the layers in the WTTES.

Fig. 20 gives an example that illustrates an optimal thermocline condition of the WTTES, in which the plotted data were collected from Scenario *5 d* from February 06 to March 02 of 2018. As shown in Fig. 20 (c), the original heat load ranged from 4 MW to 14 MW during the presented period. However, after the load shifting by the WTTES, the heat load was almost constant at around 7 MW. To achieve this flattened heat load, the WTTES adjusted its operation strategies based on the heat load conditions and the whole period was divided into four subperiods. From February 06 to February 18, the WTTES might work for peak load shaving or valley filling depending on the heat load condition. However, as shown in Fig. 20 (a), the charging process dominated the period, which featured a rising water temperature in the tank. In addition, as illustrated in Fig. 20 (b), a thermocline was gradually formulated and enhanced around Layer 2, which was indicated by increasing dimensionless temperature gaps between the layers above and below it. Moreover, the position of the thermocline was at the lower side of the tank, therefore, more space was available to store the hot water above it. From February 18 to February 21, the WTTES serviced for peak load shaving, as shown in Fig. 20 (c). This period demanded a continually discharging process, and thus the water temperature in the tank was decreased as observed in Fig. 20 (a). Moreover, opposite to the charging dominated process in the previous period, the thermocline attenuated with reducing dimensionless temperature gaps, as observed in Fig. 20 (b). The following two periods, from February 21 to February 25 and from February 25 to March 02, repeated the above two periods with a charging dominated process and a discharging dominated process, which was characterised by an enhanced and attenuated thermocline, respectively.

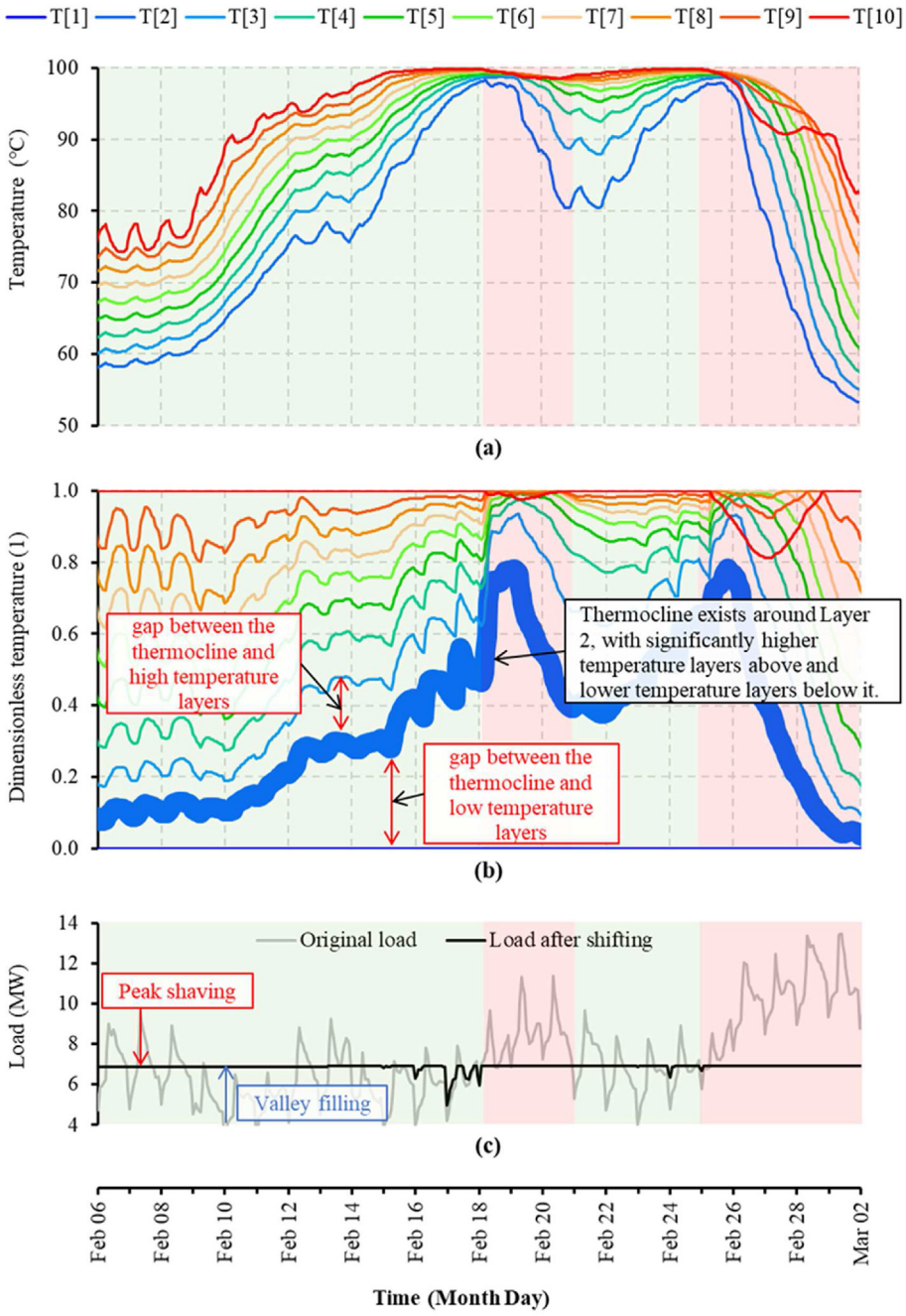


**Fig. 20.** An example of the charging and discharging processes of the WTTES, T [10] to T [1] refers to the water temperature from the top layer to the bottom layer, (a) temperature, (b) dimensionless temperature, and (c) heat load.

Some recommendations from the investigation of the thermocline of the WTTES are summarized as follows. Firstly, thermocline can be used as an effective indicator to understand the conditions and forecast the performance of WTTESs. Secondly, both the thickness and position are important to evaluate the conditions of the thermocline.

## 6. Conclusions

This study aimed to optimize prosumers' economic performance under the current unidirectional heating price models by using short-term TESs. A WTTES was chosen as the short-term TES and integrated into the prosumer. A dynamic optimization problem was formulated to explore the economic potential of the prosumer with TES. The size parameters of the TESs were swept to obtain the optimal storage size considering the trade-off between the payback period and the heating cost saving. The proposed method was tested on a campus DH system in Trondheim, Norway.

Results showed that by introducing the WTTES into the heat prosumer, the peak load was shaved by up to 39%, and the waste heat self-utilization rate was increased from 79% to 96%. These significantly improved the economic performance of the heat prosumer during the transformation period of the DH system. The annual heating cost was saved up to 1.9 million NOK, a saving of 9%, meanwhile, the initial investment of the WTTES was able to be fully recovered in less than ten years.

In addition, the effects of the peak load definition on the economic performance of the heat prosumers were discussed. It was found that the prosumers' economic performance was much better when using the hourly method to define the peak load instead of the daily method. Therefore, it was recommended that prosumers should consider the potential economic risk of introducing WTTES when the daily method is used in the heating contract. Moreover, research results highlighted the importance of the thermocline and showed that an optimal thermocline condition can lead to the high performance of the WTTES.

This study may provide guidelines on improving the heat prosumers' economic performance during the transformation period of the DH system, and hence promote the development of prosumers in DH systems.

## Declaration of competing interest

The authors declare that they have no known competing financial interests or personal relationships that could have appeared to influence the work reported in this paper.

## Acknowledgement

The authors gratefully acknowledge the support from the Research Council of Norway through the research project understanding behaviour of district heating systems integrating distributed sources under the FRIPRO/FRINATEK program (project number 262707) and the innovation project low-temperature thermal grids with surplus heat utilization under the EnergiX program (project number 280994).

## Appendix A. Setting for the case study

**Table A 1**
Parameter setting for the simulation.

| Category | Parameter | Value |
|---|---|---|
| WTTES and ground | $U$ | 1.2 W/(m$^2$ ·K) |
| | $T_{oa,aver}$ | 5.0 °C |
| | $T_{peak}$ | 4.5 °C |
| | $T_{peri}$ | 31,536,000 s |
| | $k$ | 2.7 W/(m ·K) |
| | $\rho$ | 2800 kg/(m$^3$) |
| | $C$ | 840 J/(K ·kg) |
| | $\phi$ | 4.25 rad |
| Pipeline | $L$ | 1500 m |
| | $d$ | 0.273 m |
| | $D$ | 0.4 m |
| | $h$ | 1.2 m |
| | $s$ | 1.2 m |
| | $\lambda$ | 1.5 W/(m ·K) |
| | $\lambda_i$ | 0.03 W/(m ·K) |
| Buildings | $C_{env}$ | 45,000,000,000 J/K |
| | $C_{ia}$ | 1,300,000,000 J/K |
| | $C_{ma}$ | 2,900,000,000 J/K |
| | $R_{i,e}$ | 1.18 (m$^2$ ·K)/W |
| | $R_{o,e}$ | 1.03 (m$^2$ ·K)/W |
| | $R_{i,m}$ | 0.35 (m$^2$ ·K)/W |
| | $R_{win}$ | 0.48 (m$^2$ ·K)/W |
| | $\dot{Q}_{ven}$ | 0-8,000,000 W |
| | $\dot{Q}_{in}$ | 0-4,500,000 W |
| | $\dot{Q}_{DHW}$ | 0-1,200,000 W |

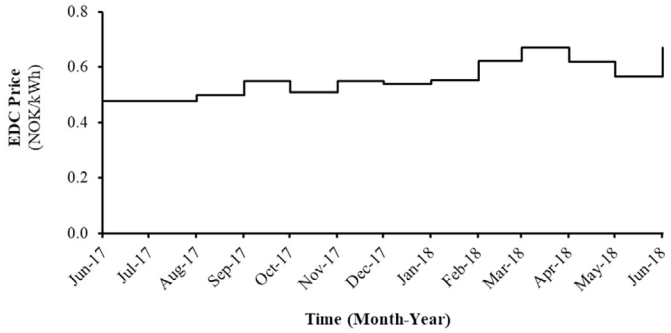


**Fig. A 1.** The EDC heating price [51]

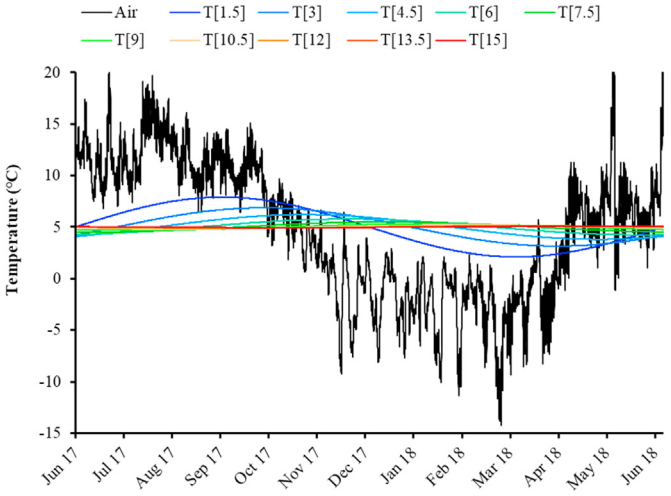


**Fig. A 2.** Measured air temperature and estimated ground temperature of the simulation year, T [15] to T[1.5] refers to the ground temperature from the 15 m depth to 1.5 m depth

## Author statement

Haoran Li: Conceptualization, Methodology, Software, Validation, Writing – original draft Juan Hou: Conceptualization, Methodology, Writing – original draft Zhiyong Tian: Writing – review & editing Tianzhen Hong: Conceptualization, Writing – review & editing Natasa Nord: Conceptualization, Writing – review & editing, Supervision Daniel Rohde: Software, Writing – review & editing

## References

[1] In focus: Energy efficiency in buildings, https://ec.europa.eu/info/news/focus-energy-efficiency-buildings-2020-feb-17en#:∼:text=Collectively%2C%20buildings%20in%20the%20EU,%2C%20usage%2C%20renovation%20and%20demolition, accessed September 2020.
[2] Heating and cooling, https://ec.europa.eu/energy/topics/energy-efficiency/heating-and-cooling_en?redir=1, accessed September 2020.
[3] Mapping and analyses of the current and future (2020-2030) heating/cooling fuel deployment (fossil/renewables), https://ec.europa.eu/energy/studies/mapping-and-analyses-current-and-future-2020-2030-heatingcooling-fuel-deployment_en, accessed September 2020.
[4] Li H, Nord N. Transition to the 4th generation district heating - possibilities,

bottlenecks, and challenges. Energy Procedia 2018;149:483–98.
[5] Sayegh MA, Danielewicz J, Nannou T, Miniewicz M, Jadwiszczak P, Piekarska K, et al. Trends of European research and development in district heating technologies. Renew Sustain Energy Rev 2017;68:1183–92.
[6] Åberg M, Fälting L, Lingfors D, Nilsson AM, Forssell A. Do ground source heat pumps challenge the dominant position of district heating in the Swedish heating market? J Clean Prod 2020;254:120070.
[7] Connolly D, Lund H, Mathiesen BV, Werner S, Möller B, Persson U, et al. Heat Roadmap Europe: combining district heating with heat savings to decarbonise the EU energy system. Energy Pol 2014;65:475–89.
[8] Werner S. International review of district heating and cooling. Energy 2017;137:617–31.
[9] Buffa S, Cozzini M, D'Antoni M, Baratieri M, Fedrizzi R. 5th generation district heating and cooling systems: a review of existing cases in Europe. Renew Sustain Energy Rev 2019;104:504–22.
[10] Christian Holmstedt Hansen OG, Hanne Kortegaard Støchkel, Detlefsen Nina. The competitiveness of district heating compared to individual heating. 2018.
[11] Dalla Rosa A, Li H, Svendsen S, Werner S, Persson U, Ruehling K, et al. IEA DHC Annex X report:Toward 4th generation district heating. Experience and Potential of Low-Temperature District Heating; 2014.
[12] Persson U, Werner S. Heat distribution and the future competitiveness of district heating. Appl Energy 2011;88(3):568–76.
[13] Nord N, Shakerin M, Tereshchenko T, Verda V, Borchiellini R. Data informed physical models for district heating grids with distributed heat sources to understand thermal and hydraulic aspects. Energy 2021;222:119965.
[14] Lickleder T, Hamacher T, Kramer M, Perić VS. Thermohydraulic model of Smart Thermal Grids with bidirectional power flow between prosumers. Energy 2021;230:120825.
[15] Marguerite C, Schmidt R-R, Pardo Garcia N. Concept development of an industrial waste heat based micro DH network. Conference Concept development of an industrial waste heat based micro DH network. LESO-PB, EPFL, p. 597-602.
[16] Pipiciello M, Caldera M, Cozzini M, Ancona MA, Melino F, Di Pietra B. Experimental characterization of a prototype of bidirectional substation for district heating with thermal prosumers. Energy 2021;223:120036.
[17] Nielsen S, Möller B. Excess heat production of future net zero energy buildings within district heating areas in Denmark. Energy 2012;48(1):23–31.
[18] Brand L, Calvén A, Englund J, Landersjö H, Lauenburg P. Smart district heating networks – a simulation study of prosumers' impact on technical parameters in distribution networks. Appl Energy 2014;129:39–48.
[19] Gross M, Karbasi B, Reiners T, Altieri L, Wagner H-J, Bertsch V. Implementing prosumers into heating networks. Energy 2021;230:120844.
[20] Huang P, Copertaro B, Zhang X, Shen J, Löfgren I, Rönnelid M, et al. A review of data centers as prosumers in district energy systems: renewable energy integration and waste heat reuse for district heating. Appl Energy 2020;258:114109.
[21] Kauko H, Kvalsvik KH, Rohde D, Nord N, Utne Å. Dynamic modeling of local district heating grids with prosumers: a case study for Norway. Energy 2018;151:261–71.
[22] Song J, Wallin F, Li H. District heating cost fluctuation caused by price model shift. Appl Energy 2017;194:715–24.
[23] Tian Z, Perers B, Furbo S, Fan J. Thermo-economic optimization of a hybrid solar district heating plant with flat plate collectors and parabolic trough collectors in series. Energy Convers Manag 2018;165:92–101.
[24] Shah SK, Aye L, Rismanchi B. Seasonal thermal energy storage system for cold climate zones: a review of recent developments. Renew Sustain Energy Rev 2018;97:38–49.
[25] Köfinger M, Schmidt RR, Basciotti D, Terreros O, Baldvinsson I, Mayrhofer J, et al. Simulation based evaluation of large scale waste heat utilization in urban district heating networks: optimized integration and operation of a seasonal storage. Energy 2018;159:1161–74.
[26] Rohde D, Andresen T, Nord N. Analysis of an integrated heating and cooling system for a building complex with focus on long–term thermal storage. Appl Therm Eng 2018;145:791–803.
[27] Rohde D, Knudsen BR, Andresen T, Nord N. Dynamic optimization of control setpoints for an integrated heating and cooling system with thermal energy storages. Energy 2020;193:116771.
[28] Verrilli F, Srinivasan S, Gambino G, Canelli M, Himanka M, Del Vecchio C, et al. Model predictive control-based optimal operations of district heating system with thermal energy storage and flexible loads. IEEE Trans Autom Sci Eng 2017;14(2):547–57.
[29] Verda V, Colella F. Primary energy savings through thermal storage in district heating networks. Energy 2011;36(7):4278–86.
[30] Harris M. Thermal energy storage in Sweden and Denmark: potentials for technology transfer. IIIEE Master thesis; 2011.
[31] The Modelica Association, https://www.modelica.org/, accessed Jan 2021.
[32] Åkesson J, Gäfvert M, Tummescheit H. Jmodelica—an open source platform for optimization of modelica models. Conference Jmodelica—an open source platform for optimization of modelica models.
[33] Amrit R, Rawlings JB, Biegler LT. Optimizing process economics online using model predictive control. Comput Chem Eng 2013;58:334–43.
[34] Nocedal J, Wright S. Numerical optimization. Springer Science & Business Media; 2006.
[35] Sernhed K, Gåverud H, Sandgren A. Customer perspectives on district heating price models. International Journal of Sustainable Energy Planning and Management 2017;13:47–60.
[36] Song J, Wallin F, Li H, Karlsson B. Price models of district heating in Sweden. Energy Procedia 2016;88:100–5.
[37] Bott C, Dressel I, Bayer P. State-of-technology review of water-based closed seasonal thermal energy storage systems. Renew Sustain Energy Rev 2019;113:109241.
[38] Pinel P, Cruickshank CA, Beausoleil-Morrison I, Wills A. A review of available methods for seasonal storage of solar thermal energy in residential applications. Renew Sustain Energy Rev 2011;15(7):3341–59.
[39] Li H, Hou J, Hong T, Ding Y, Nord N. Energy, economic, and environmental analysis of integration of thermal energy storage into district heating systems using waste heat from data centres. Energy 2021;219:119582.
[40] Powell KM, Edgar TF. An adaptive-grid model for dynamic simulation of thermocline thermal energy storage systems. Energy Convers Manag 2013;76:865–73.
[41] Li H, Hou J, Nord N. Using thermal storages to solve the mismatch between waste heat feed-in and heat demand: a case study of a district heating system of a university campus. 2019.
[42] He P, Sun G, Wang F, Wu H, Wu X. Heating engineering (in Chinese). China Architecture & Building Press; 2009.
[43] CEN. CEN/TR16355 Recommendations for prevention of Legionella growth in installations inside buildings conveying water for human consumption. 2012.
[44] Frederiksen S, Werner S. District heating and cooling. Studentlitteratur Lund; 2013.
[45] Andújar Márquez JM, Martínez Bohórquez MÁ, Gómez Melgar S. Ground thermal diffusivity calculation by direct soil temperature measurement. Application to very low enthalpy geothermal energy systems. Sensors 2016;16(3):306.
[47] Jaluria Y. Design and optimization of thermal systems. CRC press; 2007.
[48] Nord N, Sandberg NH, Ngo H, Nesgård E, Woszczek A, Tereshchenko T, et al. Future energy pathways for a university campus considering possibilities for energy efficiency improvements. Conference Future energy pathways for a university campus considering possibilities for energy efficiency improvements, vol. vol. 352. IOP Publishing, p. 012037.
[49] Guan J, Nord N, Chen S. Energy planning of university campus building complex: energy usage and coincidental analysis of individual buildings with a case study. Energy Build 2016;124:99–111.
[50] Cruickshank CA. Evaluation of a stratified multi-tank thermal storage for solar heating applications. Doctoral thesis; 2009.
[51] Charging method for heating bill in Trondheim, https://www.statkraftvarme.no/globalassets/2-statkraft-varme/statkraft-varme-norge/om-statkraft-varme/prisark/20190901/fjernvarmetariff-trondheim-bt1.pdf, accessed September 2020.
[52] Mangold D, Deschaintre L. Task 45 Large Systems Seasonal thermal energy storage Report on state of the art and necessary further R+ D. International Energy Agency Solar Heating and Cooling Programme; 2015.
[53] ASHRAE. ASHRAE guideline 14–2014, measurement of energy, demand, and water savings. ASHRAE Atlanta; 2014.
[54] Larsson O. Pricing models in district heating. Master thesis; 2011.
[55] Li G. Sensible heat thermal storage energy and exergy performance evaluations. Renew Sustain Energy Rev 2016;53:897–923.
[56] Ghaddar NK. Stratified storage tank influence on performance of solar water heating system tested in Beirut. Renew Energy 1994;4(8):911–25.